

Assesment of liver blood flow using a navigator echo respiratory gated parallel imaging technique at 1.5 T

L. S. Truica^{1,2}, and I. Cameron²

¹Carleton University, Ottawa, ON, Canada, ²Diagnostic Imaging - MRI research Lab, Ottawa Hospital- General Campus

Introduction: Motion related artifacts have limited the usefulness of diffusion weighted imaging (DWI) of abdominal organs and for the evaluation of abdominal pathology in the past. A few studies have shown that liver blood flow can be assessed with DWI^{1,2} however, there is a need for improved acquisition and analysis tools. The results reported here were acquired with both a breath hold (BH) sequence, as well as with a parallel imaging and respiratory triggered non-breath hold sequence (FB). To our knowledge there are no reports of intravoxel incoherent motion model (IVIM) studies of the liver that used a navigator echo respiratory triggered sequence.

Methods: Imaging was done on a Siemens Symphony-TIM 1.5 T scanner with 30 mT/m gradients. 18 normal liver volunteers (21 to 61 yrs old) were recruited. The study had IRB approval and informed consent was received from all subjects. DWI of the entire liver was done for 8 subjects and artifact free images using a navigator echo respiratory triggered DW_SS EPI sequence were obtained: TR=3080-5866 ms, TE=94 ms, FOV=350-450 mm, phase FOV=75%, 144x192 matrix, iPAT-GRAPPA factor=2, eighteen 10 mm thick axial slices (2.5mm gap), total imaging time=124 s, diffusion gradients were in the slice select direction, spectral fat saturation was used and 13 *b*-values: 0, 50, 100, 150, 200, 250, 300, 350, 400, 450, 500, 650, 800 s/mm² for FB part of the study. Before the TIM upgrade of the MR scanner DW images of 3 subjects were acquired with the BH protocol for all *b*-values, during a single 30 to 35 s breath hold depending on the number of slices acquired; a DW single-shot echo-planar-imaging (DW SS EPI) sequence was used: TR = 2500 ms, TE = 91 ms, 4 to 6 axial 10 mm axial slices, 2.5 mm gap, NEX = 1, FOV = 380 mm, phase FOV = 75%, 128x96 matrix, total imaging time of 30 to 35 s, Spectral fat saturation was used to suppress chemical shift artefacts and 10 *b*-values: 0, 10, 20, 30, 50, 90, 150, 300, 500 and 800 s/mm² was used.

Analysis: Analysis was performed in the same manner for both the BH and FB protocols. Data analysis assumed the IVIM model^{3,4,5}, which considers water diffusion and blood microcirculation as separate components of the diffusion decay:

$$S / S_0 = (1 - f) \exp(-bD) + f \exp(-bD^*) \quad [1]$$

where *S* is the DW signal, *S*₀ is the *b*=0 signal, *D* and *D*^{*} are the diffusion and pseudo-diffusion coefficients, respectively, and *f* is the perfusion fraction. Diffusion decays for 3 100-pixel rectangular ROIs were fit to Eq 1 to evaluate *D*, *f*, and *D*^{*}. The ROIs were positioned carefully to avoid areas where large blood vessels are present. In a separate analysis a larger ROI was drawn around the whole liver. *D*, *D*^{*} and *f* maps were calculated pixel-by-pixel and color overlaid onto an anatomical image.

Results and Discussion: For the BH-protocol only 3 subjects were reported (10 subjects scanned) because of strong chemical shift and/or motion artifacts on many of the images. Fig 1 shows the fit parameters for whole right liver (WRL-ROI) and 100-pixel ROIs (PRL-ROIs) vs. volunteers. The WRL-ROI and PRL-ROI results were in good agreement for both breathing protocols. To within experimental error, the same IVIM parameter values are obtained for the PRL-ROI and the WRL-ROI, even though the positioning of the three 100-pixel ROIs was done very carefully to avoid large vessels while no such precaution was taken for the ROI drawn to encompass the whole right liver side. This concludes that there are no gradual variations across the liver, this excluding the areas that contain large blood vessels. The intra and inter-subject variability for all IVIM parameters, including *D*^{*}, is higher for the BH-protocol clearly suggesting that the deficiencies of the BH protocol and the hardware used for these measurements outweigh the benefit of having small *b*-values. Fig 2 shows color maps of *f*, *D*^{*} and *D*. The range on the color table is: a) *f* (0-100)%, b) *D*^{*} (0-200) x10⁻³mm²/s and c) *D* (0-2) x10⁻³mm²/s. The variation of *f* and *D*^{*} across the liver on the color parametric maps is consistent with the anatomy of the liver. Higher *D*^{*} values can be seen around larger blood vessels ~ brighter areas on Fig. 2(right) ~where, since they are collecting or spreading blood, a higher blood flow is expected and a constant behaviour is observed for the rest of the liver. To within experimental error, all patients had the same values of *D* (1.10 mm²/s ± 0.16 mm²/s), *D*^{*} (46 mm²/s ± 17 mm²/s) and *f* (44.0% ± 6.9%) in liver for the FB protocol and *D* (1.13 mm²/s ± 0.22 mm²/s), *D*^{*} (70 mm²/s ± 19 mm²/s) and *f* (34.0% ± 11%) for the BH protocol.

Conclusion: The improvements in data acquisition and analysis presented in this study provided more consistent results for *f*, *D*^{*} and *D* for normal liver than previously reported studies in both FB and BH approaches. Parametric maps of *f* and *D*^{*} were consistent with blood flow patterns in liver⁶. Fit parameter maps can be a useful tool in identifying differences in tissues and give important insight into the hemodynamic system of interest. This technique could become instrumental in the assessment and management of normal or diseased tissue in the abdomen. The use of parallel imaging in combination with modern phased array coils leads to a considerable improvement in the quality of the data.

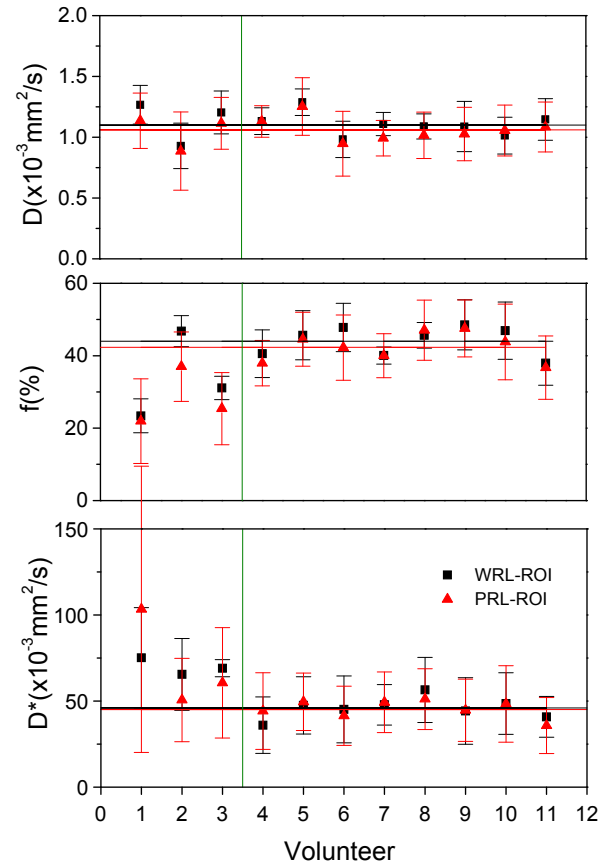


Fig 1 Fit parameters values (mean ± SD) for the WRL-ROI, the three 100-pixel ROIs and the PRL-ROI, averaged over all slices in each case. The olive line separates the BH-protocol volunteers (1 to 3) of the FB-protocol volunteers (4 to 11). The horizontal lines show the mean over all volunteers scanned with the FB-protocol for the PRL-ROI (red) and the WRL-ROI (black).

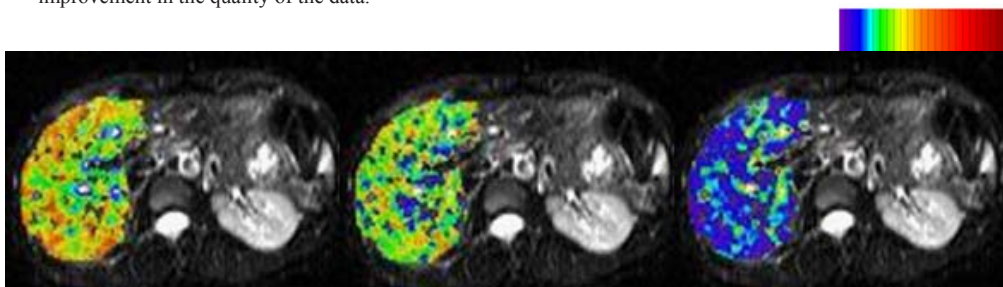


Fig 2 Maps: *f* (left), *D* (center) and *D*^{*} (right)

References:

1. Yamada et al., Radiology 1999;210:617-623
2. Luciani et al., Radiology 2008;249(3):891-899
3. Le Bihan et al, Magn Reson Q 1991; 7:1-30
4. Le Bihan et al, Radiology 1988; 168:497-505
5. Le Bihan et al, J. Com. Ass. To. 1991; 15:19-25
6. Gray H, Anatomy of the Human Body, 15th Edition, Chancellor Press, 1994